The action of pressure-radiation forces on pulsating vapor bubbles

Y. Hao, H. N. Oğuz, and A. Prosperetti[a)]
Department of Mechanical Engineering, The Johns Hopkins University, Baltimore, Maryland 21218

(Received 29 February 2000; accepted 22 January 2001)

The action of pressure-radiation (or Bjerknes) forces on gas bubbles is well understood. This paper studies the analogous phenomenon for vapor bubbles, about which much less is known. A possible practical application is the removal of boiling bubbles from the neighborhood of a heated surface in the case of a downward facing surface or in the absence of gravity. For this reason, the case of a bubble near a plane rigid surface is considered in detail. It is shown that, when the acoustic wave fronts are parallel to the surface, the bubble remains trapped due to secondary Bjerknes force caused by an ''image bubble.'' When the wave fronts are perpendicular to the surface, on the other hand, the bubble can be made to slide laterally. © *2001 American Institute of Physics.*
[DOI: 10.1063/1.1359746]

I. INTRODUCTION

At normal gravity, the effectiveness of boiling as a heat transfer mechanism relies in no small measure on the rapid removal of vapor bubbles from the heated surface. This process has a twofold benefit, as it both aids in removing latent heat, and in promoting microconvective motion near the surface. On the basis of this remark, one would expect that boiling at reduced gravity would be very inefficient. Somewhat surprisingly, at small to moderate heat fluxes, several experiments have shown this not to be the case (see, e.g., Refs. 1–4). Since bubbles do not leave the vicinity of the heated surface, they coalesce and give rise to a large vapor cavity.[5] The coalescence of the newly formed bubbles with this cavity is accompanied by surface instabilities[6] and vigorous convection, which are able to maintain a relatively large degree of heat transfer.

While, for this reason, the hovering of large bubbles near the nucleation sites is beneficial at low to moderate heat fluxes, it is also at the root of an observed large reduction in critical heat flux with respect to normal gravity conditions, as the cavity becomes so large as to envelop the heating surface.[4,7] In order to increase the critical heat flux at low gravity it is therefore desirable to remove bubbles from the heated surface by providing a substitute for buoyancy. A similar problem is encountered at normal gravity with downward-facing heating surfaces. The techniques available for this purpose include flow, electric, and acoustic fields. The usefulness of flow is limited as, due to the no-slip condition at the solid surface, relatively large flow velocities are required to effectively remove bubbles, which renders this option impractical. The usefulness of electric fields is currently under consideration by several groups (see, e.g., Refs. 8–10). Here we focus on the action of acoustic pressure forces (also known as Bjerknes forces) on vapor bubbles as a means to achieve this end.

The action of acoustic radiation forces on gas—rather than vapor—bubbles is well known (see, e.g., Refs. 11–22). For example, radiation forces are a major factor in acoustic cavitation where they promote violent translational motion and spatial reorganization of the gas that evolves from the liquid in an intense sound field. These and other aspects of pressure radiation forces have been extensively studied both experimentally and theoretically (see, e.g., Refs. 23–28). Gas bubbles are attracted or repelled by the pressure antinodes according to whether they are driven below or above their resonance frequency. Furthermore, in the linear regime, neighboring bubbles repel each other when one is driven above and one below the natural frequency while they attract otherwise.

While this information gives some insight into what to expect in the case of vapor bubbles, with the latter the situation is so different that a specific study is required. Indeed, vapor bubble dynamics is so strongly dependent on heat transfer with the liquid that the very concept of equilibrium radius becomes essentially inapplicable, even as an approximation. Furthermore, when the bubble starts translating under the action of the pressure force, the vapor–liquid heat transfer is drastically altered.

In this paper we consider a spherical vapor bubble in the vicinity of a plane rigid surface. The assumption of sphericity is of course questionable near a solid surface which is well known to promote deformation and jetting in the bubble during the contraction phase of the pulsations (see, e.g., Refs. 29–31). Nevertheless, since pressure-radiation forces couple to volume changes and are, therefore, little sensitive to the bubble shape, for moderate sound fields, one would not expect it to introduce qualitative differences in the bubble response and it is therefore a useful starting point to sort out the basic features of this complex phenomenon.

The vicinity of the bubble is subjected to a standing acoustic wave which causes it to pulsate as well as to trans-

[a)]Also at Department of Applied Physics, Twente Institute of Mechanics, and Burgerscentrum, University of Twente, AE 7500 Enschede, The Netherlands.

late. Since the flow is assumed potential, the effect of the wall can be replaced by that of an ''image'' bubble which, being always in phase with the real one, exerts an attractive force. The motion of the bubble therefore takes place under the direct action of the imposed sound field (the so-called primary Bjerknes force) and of the attractive force of the image bubble (the secondary Bjerknes force). This circumstance makes for a variety of possible behaviors as will be seen in the following.

II. MATHEMATICAL FORMULATION

We consider a pulsating and translating spherical bubble in the neighborhood of a plane rigid wall. Even a simplified mathematical model of this situation is a matter of some complexity as it requires a description of the bubble dynamics, the evaluation of the energy transfer, and the calculation of the velocity and pressure fields. We address these aspects in turn and give some additional details in the appendices.

A. Flow fields

It is shown in Appendix A that, when the Mach number of the flow induced by the bubble is small, if viscous effects are neglected, the problem can be reduced to the standard incompressible form

$$\nabla^2\phi=0, \tag{2.1}$$

$$\frac{\partial\phi}{\partial t}+\frac{1}{2}\mathbf{u}^2+\frac{P_L}{\rho_L}=\frac{P_\infty+P_A}{\rho_L}, \tag{2.2}$$

where P_∞ is the static pressure, and the driving acoustic field P_A is evaluated in the neighborhood of the instantaneous position of the bubble center $\mathbf{x}_B(t)$; the liquid density is denoted by ρ_L, ϕ is the harmonic velocity potential, and P_L is the liquid pressure.

In order to describe the fluid-dynamic interaction of two (or more) spherical bubbles in a potential flow we use the method of Sangani and co-workers,[32,33] which, following Ref. 34, is here extended to the case of bubbles with a variable radius. More details are given in Ref. 49 of this paper available as AIP Document No. E-PHFLE6-13-009105, which may be retrieved via the EPAPS homepage `http://www.aip.org/pubservs/epaps.html`.[49]

In a neighborhood of the bubble, ϕ may be expressed as a superposition of multipoles:

$$\begin{aligned}\phi&=\sum_{n=0}^{\infty}\sum_{m=0}^{n}\left\{\left[C_{nm}r^n+D_{nm}\frac{R^{2n+1}}{r^{n+1}}\right]Y_n^m\right.\\&\left.\quad+\left[\tilde{C}_{nm}r^n+\tilde{D}_{nm}\frac{R^{2n+1}}{r^{n+1}}\right]\tilde{Y}_n^m\right\}\\&\equiv\sum_{n=0}^{\infty}\sum_{m=0}^{n}\left[f_{nm}(r)Y_n^m+\tilde{f}_{nm}(r)\tilde{Y}_n^m\right],\end{aligned} \tag{2.3}$$

where

$$Y_n^m=P_n^m(\cos\theta)\cos m\phi,\quad \tilde{Y}_n^m=P_n^m(\cos\theta)\sin m\phi, \tag{2.4}$$

with P_n^m associated Legendre functions, are spherical harmonics. The system of spherical coordinates (r,θ,ϕ) is centered at the instantaneous position of the bubble center, with the polar axis normal to the solid wall. The instantaneous bubble radius is denoted by $R=R(t)$.

At the bubble surface we impose the kinematic boundary condition

$$\mathbf{n}\cdot\nabla\phi=\dot{R}(t)+\mathbf{n}\cdot\mathbf{w}(t), \tag{2.5}$$

where $\mathbf{n}$ is the unit outward normal and $\mathbf{w}$ the bubble translational velocity; here and in the following dots denote time derivatives. As a consequence, one readily finds that

$$D_{00}=-R\dot{R}, \tag{2.6}$$

$$2D_{10}-C_{10}=-w_1,\quad 2D_{11}-C_{11}=w_2,\quad 2\tilde{D}_{11}-\tilde{C}_{11}=w_3, \tag{2.7}$$

while, for $2\leqslant n$, $0\leqslant m$,

$$nC_{nm}-(n+1)D_{nm}=0,\quad n\tilde{C}_{nm}-(n+1)\tilde{D}_{nm}=0. \tag{2.8}$$

The remaining coefficients must be determined by imposing the kinematic condition on the rigid wall. Within the framework of potential flow the easiest way to accomplish this task is to introduce an image bubble in the neighborhood of which the potential is described by an expression similar to (2.3). The requirement that these two expansions describe the same function in the region where they are both valid determines a series of relations among the coefficients which are given in explicit form in Ref. 49. With this step, the potential is entirely determined in terms of the bubble radius and radial and translational velocities. The equations that determine these quantities are given later in Sec. II D.

B. Energy equation

The bubble internal pressure is strongly dependent on the surface temperature that must be determined by solving the liquid energy equation

$$\frac{\partial T_L}{\partial t}+(\nabla\phi)\cdot\nabla T_L=D_L\nabla^2T_L, \tag{2.9}$$

where T_L is the liquid temperature and D_L the liquid thermal diffusivity. This equation should be solved subject to the condition that, at $r=R(t)$, the liquid temperature is equal the local bubble surface temperature T_S. In principle it would be necessary to allow for surface temperature nonuniformities, but it is well known that such effects are very small due to the rapidity with which local processes of evaporation and condensation are able to erase temperature differences inside the bubble. Hence we assume that T_S is uniform over the bubble surface.

In the present model the liquid is isothermal except for the effect of the bubble. Thus, the region adjacent to the bubble where the liquid temperature is strongly nonuniform only extends over a thickness of the order of a few thermal penetration lengths $\sqrt{D_L/\omega}$ which, for water at 1 kHz, is of the order of tens of micrometers. For this reason, in the situ-

ations considered here, it is possible to neglect the thermal interaction of the bubble with the wall and other bubbles (be they real or images).

The approximation of a spatially uniform pressure in the bubble is well justified when, as here, the vapor velocity is small with respect to the speed of sound.[35] When, as here, the Mach number of the vapor flow is small, whether thermodynamic equilibrium conditions can be assumed to prevail at the bubble surface depends on frequency and the accommodation coefficient α. This latter quantity is notoriously difficult to measure or calculate; in particular, for water, the literature gives values as low as 0.006 and as high as 1.[36,37] If α is near the low end of the reported range, equilibrium conditions can be expected to hold for frequencies up to about 10 kHz[38–40] while, with α close to 1, equilibrium can be safely assumed all the way up to the MHz range. Several studies, including a recent molecular dynamics simulation,[41] support the larger estimates of α and, in view of the existing uncertainty and with an eye toward simplicity, we assume here thermodynamic equilibrium, especially since, in most of the examples that follow, we consider frequencies in the kHz range. Thus, we take the vapor to be in saturated conditions at the instantaneous bubble surface temperature T_S so that $p_V = p_{\mathrm{sat}}(T_S)$, $\rho_V = \rho_{\mathrm{sat}}(T_S)$ (see also Ref. 42). In a sound field, the growth rate of a bubble by rectified diffusion of heat is much faster than that by rectified diffusion of the permanent gas dissolved in the liquid. Therefore, even if the liquid is not thoroughly degassed, the bubble is predominantly filled with vapor and we neglect permanent gas effects. In some cases, noncondensibles can accumulate near the vapor–liquid interface and affect the rate of vapor condensation during the compression phase of the bubble pulsations thus leading to an even faster growth by vapor rectification. These phenomena depend on the detailed conditions under which the process takes place and, since we are here concerned with its salient features, they are neglected.

A second condition to impose on the solution of the energy equation is conservation of energy at the bubble surface. In a previous study,[43] where we allowed for a nonuniform temperature distribution in the liquid, it was shown that the vapor temperature can be considered approximately uniform throughout the bubble over a broad range of acoustic frequencies and pressure amplitudes. As a consequence, the vapor-side contribution to the interfacial energy balance is negligible and, upon averaging over the bubble surface (indicated by an overline), the conservation of energy at the interface becomes[43]

$$4\pi R^2 k_L \left.\overline{\frac{\partial T}{\partial r}}\right|_{r=R(t)} = L\frac{d}{dt}\left(\frac{4}{3}\pi R^3 \rho_V\right) + \frac{4}{3}\pi R^3 \rho_V c_s \frac{dT_S}{dt}, \tag{2.10}$$

where $c_s = c_{pV} - L/T_S$ (with c_{pV} the vapor specific heat at constant pressure) is the thermal heat capacity along the saturation line, and ρ_V the saturated vapor density. The last term in (2.10) is often omitted in the boiling literature when time scales are slow enough to make it unimportant. In the presence of an acoustic field, however, time scales can be shorter and, therefore, the time derivative significant [see, e.g., Ref. 44, Eq. (6)].

C. Radial motion

An equation for the radial motion of the bubble can be obtained by imposing the dynamic boundary condition that the liquid pressure P_L equal the bubble internal pressure with the surface tension contribution. Given the sphericity approximation that we introduced, this condition cannot be satisfied at each point of the interface, but only on average:

$$p_{\mathrm{sat}} = \overline{P}_L + \frac{2\sigma}{R}, \tag{2.11}$$

where the overline denotes the average over the bubble surface and σ is the surface tension coefficient. Upon calculating P_L from the Bernoulli integral with the potential given by (2.3), we find

$$\begin{aligned} 4\pi R^2 \frac{d}{dt}(R\dot{R} - C_{00}) - 8\pi R[f_{10}D_{10} + f_{11}D_{11} + \tilde{f}_{11}\tilde{D}_{11}] \\ = \frac{4\pi R^2}{\rho_L}\left(p_{\mathrm{sat}} - P_\infty - P_A(\mathbf{x}_B, t) - \frac{2\sigma}{R}\right) \\ - \frac{2}{3}\pi R^2(3\dot{R}^2 + \mathbf{w}\cdot\mathbf{w}) - 2\pi\sum_{n=0}^{\infty}\left[\frac{n(n+1)}{2n+1}f_{n0}^2 \right. \\ \left. + \sum_{m=1}^{n}\frac{(n+m)!}{(n-m)!}\frac{n(n+1)}{2(2n+1)}(f_{nm}^2 + \tilde{f}_{nm}^2)\right], \end{aligned} \tag{2.12}$$

where all the $f_{nm}, \tilde{f}_{nm}$ are evaluated at R.

It is shown in Ref. 49 that this equation reduces to the familiar Rayleigh–Plesset equation when the bubble is far away from the rigid boundary.

D. Translational motion

With the neglect of the mass of the bubble contents, the total force on the bubble must vanish so that, at every instant,

$$\int_S dS\, \mathbf{n} P_L = 0. \tag{2.13}$$

Since the bubble radius is assumed to be much smaller than the acoustic wavelength, P_A is a slowly varying function over the bubble surface and its contribution to the integral can be evaluated with sufficient accuracy by carrying out a Taylor series expansion centered at the bubble center $\mathbf{x}_B$. With this step, Eq. (2.13) becomes

$$\int_S dS\, \mathbf{n}(P_L - P_A) + V\nabla P_A = 0, \tag{2.14}$$

where ∇P_A is evaluated at the position of the bubble center and

$$V = \tfrac{4}{3}\pi R^3 \tag{2.15}$$

is the instantaneous bubble volume. The first term in (2.14) only contains the incompressible part of the pressure and can

be calculated by standard methods of incompressible potential flow as shown in Ref. 49. In this way the equations governing the translational motion of the bubble can be found; they are given explicitly in Ref. 49. The position of the bubble center is updated by integrating

$$\frac{d\mathbf{x}_B}{dt}=\mathbf{w}. \tag{2.16}$$

III. NUMERICAL METHOD

In order to solve the energy equation (2.9) we expand the liquid temperature T_L in a series of spherical harmonics similar to (2.3):

$$T_L=\sum_{N=0}^{\infty}\sum_{M=0}^{N}[S_{NM}(r,t)Y_N^M+\tilde{S}_{NM}(r,t)\tilde{Y}_N^M], \tag{3.1}$$

substitute into (2.9), and take scalar products with the generic spherical harmonic to find equations of the form

$$\frac{\partial S_{NM}}{\partial t}+F_C(f_{pq},S_{IJ})=\frac{D_L}{r^2}\left[\frac{\partial}{\partial r}\left(r^2\frac{\partial S_{NM}}{\partial r}\right)-N(N+1)S_{NM}\right], \tag{3.2}$$

where F_C consists of products of spatial derivatives of the f's and the S's; its explicit form is given in Appendix B. In practice, we truncate the expansion (3.1) to a maximum value N_m. The terms of order $N>N_m$ that arise due to the coupling between different harmonics are simply set to zero.

From the continuity of temperature at the bubble surface we deduce

$$S_{00}(R(t),t)=T_S(t),\quad S_{NM}(R(t),t)=0,\quad M,N\neq 0. \tag{3.3}$$

The interface energy balance (2.10) gives

$$4\pi R^2 k_L\left.\frac{\partial S_{00}}{\partial r}\right|_{r=R(t)}=L\frac{d}{dt}\left(\frac{4}{3}\pi R^3\rho_V\right)+\frac{4}{3}\pi R^3\rho_V c_s\frac{dT_S}{dt}. \tag{3.4}$$

For the reasons given in Sec. II B, far from the bubble we require that $T\to T_\infty$, and therefore

$$S_{00}\to T_\infty,\quad S_{NM}\to 0,\quad M,N\neq 0, \tag{3.5}$$

as $r\to\infty$.

Equation (3.2), written for $N=0,1,\ldots,N_m$ and the corresponding M's, constitute a system of coupled partial differential equations that is solved by a collocation method that extends the one used in our previous works.[43,45] We expand each S_{NM} in a series of even Chebyshev polynomials T_{2K}:

$$S_{NM}=\sum_{K=0}^{J}a_{NMK}(t)T_{2K}(\zeta), \tag{3.6}$$

where we have introduced the new spatial variable

$$\zeta=\frac{m}{m+r-R(t)}. \tag{3.7}$$

Here $m=\eta\sqrt{D_L/\omega}$ is taken to be a multiple η of the thermal penetration depth in the liquid $\sqrt{D_L/\omega}$; the parameter η is typically taken to be 10. The variable ζ maps the domain $R(t)\leqslant r<\infty$ exterior to the bubble to the fixed domain $1\geqslant\zeta>0$. The use of only the even Chebyshev polynomials ensures that $\partial S_{NM}/\partial r\to 0$ as $r\to\infty$.

For each S_{NM} the expansion (3.6) is substituted into (3.2) and the resulting expressions evaluated at the $J-1$ collocation points

$$\zeta_j=\cos\frac{\pi j}{2J},\quad j=1,2,\ldots,J-1. \tag{3.8}$$

At $r=R(t)$ (i.e., $\zeta=1$, $j=0$) we impose the interface boundary conditions (3.3) and (3.4) and, for $r\to\infty$ (i.e., $\zeta=0$, $j=J$), the conditions (3.5). In this way a system of ordinary differential equations sufficient for the determination of the coefficients $a_{NMK}(t)$ is generated.

Several steps have been taken to validate the computer program. In the first place, when the bubble is far from the rigid boundary, it behaves as a free bubble and its dynamics can be studied with the tools developed in our earlier studies.[43,45] We have checked that the new computer code gave results identical to those of the previous codes, which had been thoroughly validated according to the procedures described in the earlier papers. In particular, it was checked that the results for a bubble translating in the x, y, and z directions were identical. Second, for a bubble near the solid boundary, we have verified that the results were independent of the direction of translation in a plane parallel to the solid boundary. Once the accuracy of the program was ascertained in this manner, we conducted the usual convergence studies by varying the number of terms retained in the potential and temperature expansions, and in the Chebyshev expansions. Furthermore, we have also varied the number of collocation points. It was found that, for the cases depicted in Figs. 1–5, taking $n_m=2$ in the potential expansion (2.3) and $N_m=8$ in the temperature expansion (3.1) gave converged results; since these cases are all axisymmetric, $m=M=0$. For the calculation of Fig. 6 we took $n_m=2$, $m=2$, $N_m=4$, $M=4$. In all cases we used 16 terms in the Chebyshev expansion (3.6) and 16 collocation points.

IV. RESULTS: SOUND WAVE FRONTS PARALLEL TO THE SOLID SURFACE

We consider first the case in which the sound field consists of standing one-dimensional waves with the wave fronts parallel to the solid surface:

$$P_A=P_a\sin\omega t\cos kz. \tag{4.1}$$

Here P_a is acoustic pressure amplitude, ω the angular frequency, $k=\omega/c_\infty$ (with c_∞ the speed of sound in the liquid) the wave number, and z is the distance from the plane solid surface which is taken to be rigid enough to be a pressure antinode. In this case the problem is axisymmetric and all the coefficients with index $m\neq 0$ vanish; the summations over this index are therefore unnecessary and can be omitted. It can be explicitly verified that the equations given in Sec. II reduce then to the simpler axisymmetric form given in an earlier paper.[45]

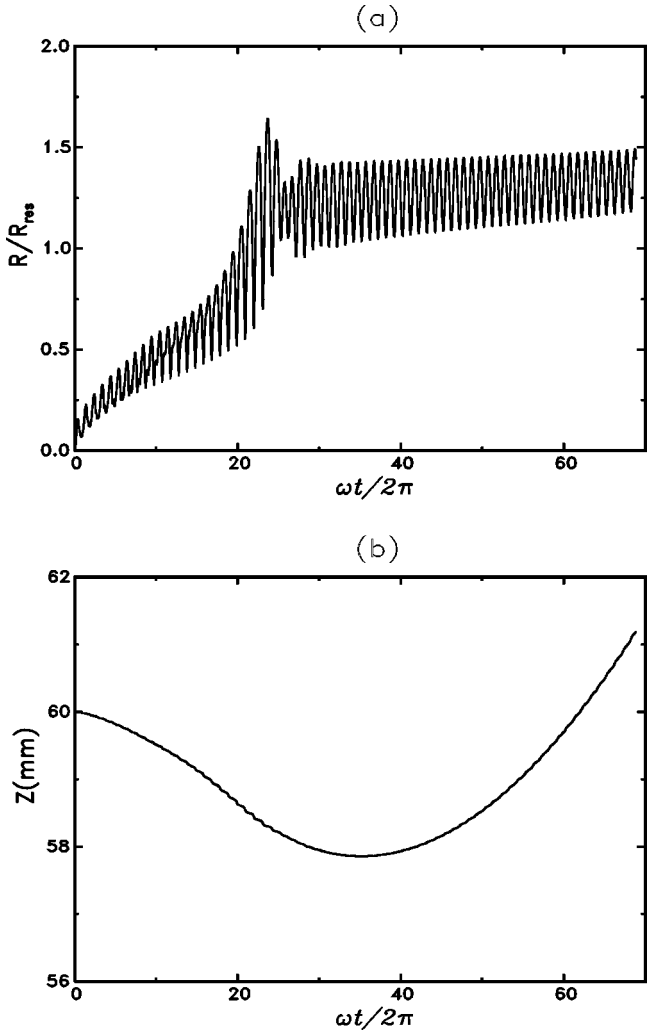

FIG. 1. Bubble radius (upper panel) and distance between the bubble center and the wall (lower panel) as functions of the number of sound cycles. Initially the bubble is located at a distance of 60 mm from the plane wall. The bubble radius is normalized by the linear resonance value R_{res} which is 2.71 mm in this case; the initial radius is 35 μm. The sound frequency is 1 kHz, the acoustic pressure amplitude 0.3 atm, and the liquid water in saturated conditions at 1 atm and 100 °C. The acoustic wave fronts are parallel to the wall.

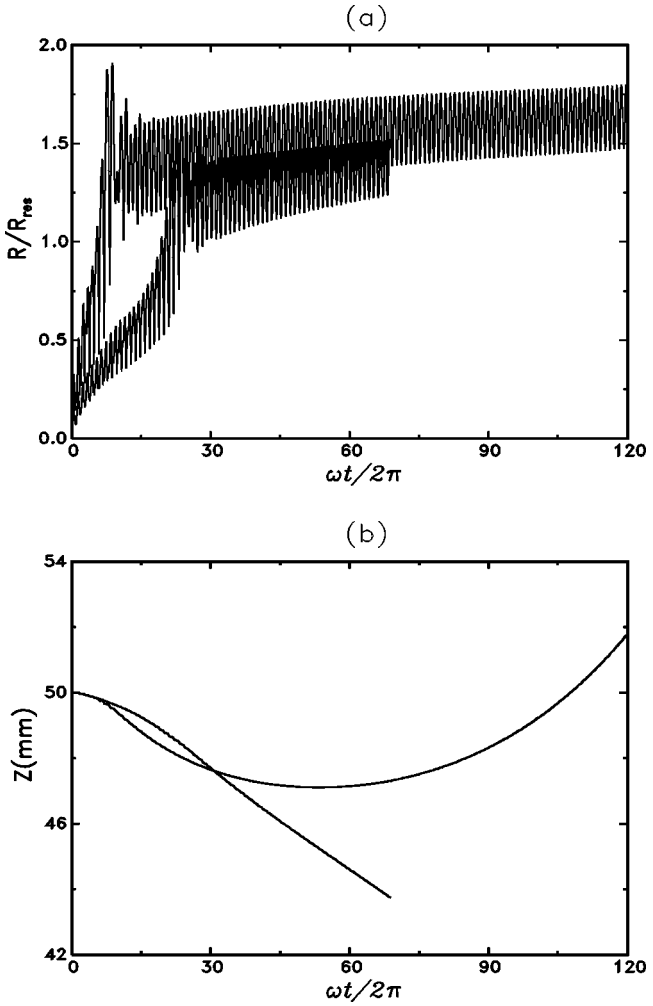

FIG. 2. Effect of the pressure amplitude on a bubble initially placed at 50 mm from the wall. At a pressure amplitude of 0.5 atm the bubble is eventually repelled by the wall while at 0.3 atm it is attracted; other conditions are as in Fig. 1.

Figures 1–3 show in the upper panel the bubble radius and in the lower panel the distance between the bubble center and the wall, both as functions of nondimensional time; the radius is normalized by the linear resonance value R_{res} (see, e.g., Ref. 43) which, in this case, equals 2.71 mm. Here the sound frequency is $\omega/2\pi=1$ kHz, the bubble is started with a radius of 35 μm in 100 °C water at 1 atm (101.3 kPa) ambient pressure. These figures show results for an acoustic pressure amplitude of $P_a=0.3$ atm (30.39 kPa); Fig. 2 also shows results for $P_a=0.5$ atm (50.65 kPa). In all cases the bubble moves initially toward the wall. For the case of Fig. 1, in which the bubble is initially sufficiently far from the wall, this motion is arrested by the reversal of the Bjerknes force and the bubble is ultimately repelled by the wall. This behavior conforms with the known nature of pressure-radiation (or Bjerknes) forces which drive bubbles in the direction of the pressure minimum at the instant at which the bubble reaches its maximum radius. In particular, bubbles driven below resonance tend to move in the direction of pressure antinodes, while above resonance the force is directed toward pressure nodes.

For an initial distance of 50 mm from the wall (Fig. 2), at the lower acoustic pressure amplitude of 0.3 atm, the bubble continues to move toward the wall even after growing past the resonance radius. This is a consequence of the combined effects of inertia and of the secondary Bjerknes force exerted by the image bubble. If the acoustic pressure is increased to 0.5 atm, however, bubble growth is faster and, when the bubble grows beyond the resonant radius, it is sufficiently far from the wall that it can be pulled away by the primary Bjerknes force. In the third example of Fig. 3, the bubble is released much closer to the wall, 10 mm away, and it essentially touches it before growing past the resonant radius. In both Figs. 2 and 3 the calculation is stopped when the bubble touches the wall.

This behavior is typical and is illustrated in Figs. 4 and 5 for a higher sound frequency, $\omega/2\pi=20$ kHz; the resonant radius is now 75 μm and the initial radius 35 μm as before;

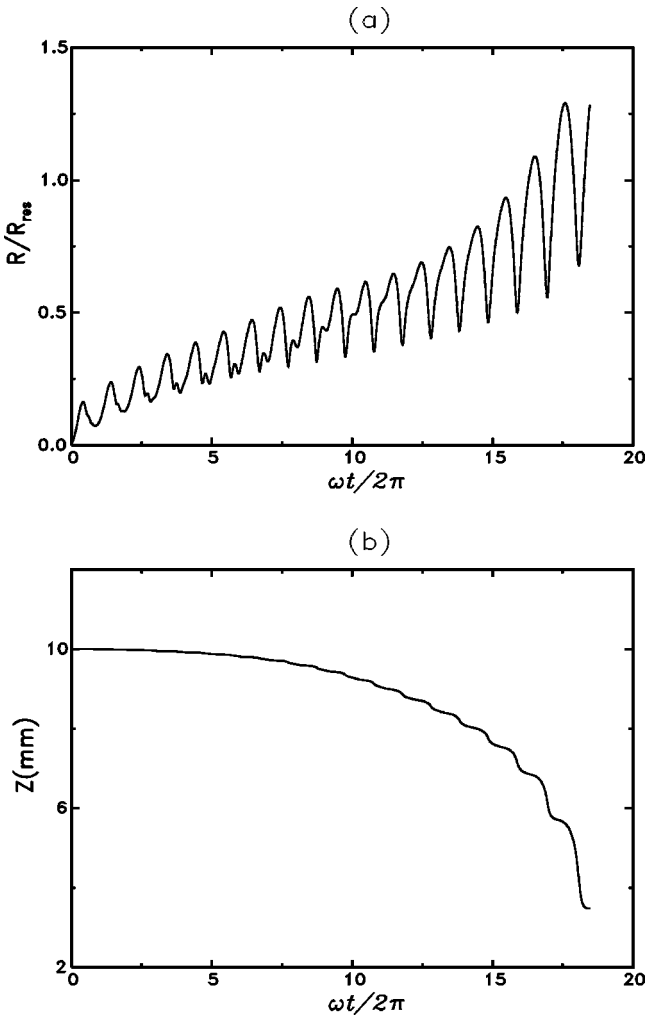

FIG. 3. The same as in Fig. 1 for an initial bubble position 10 mm from the wall.

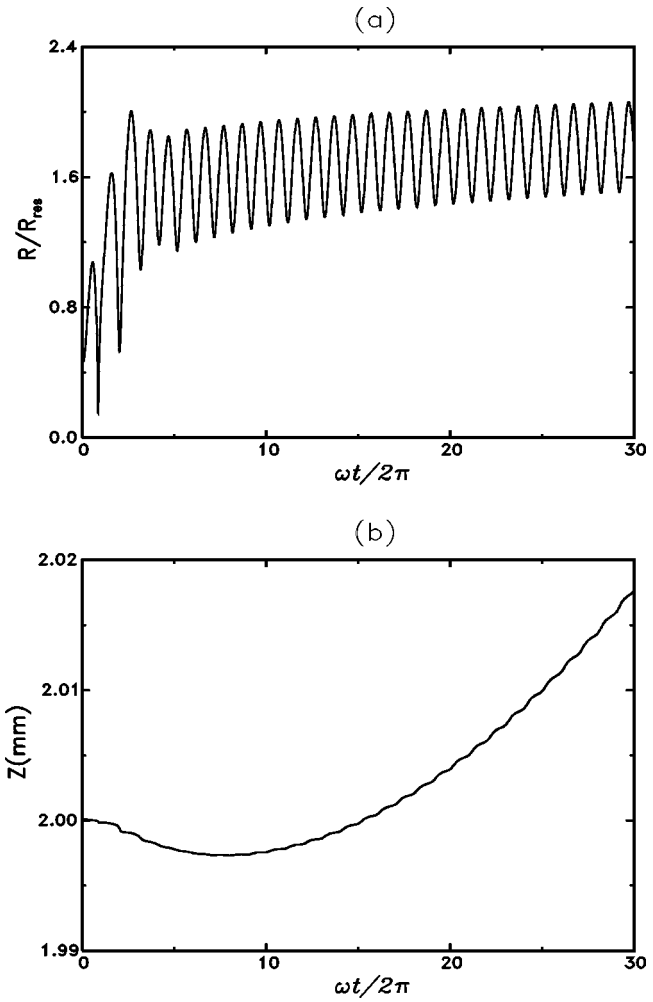

FIG. 4. Bubble radius (upper panel) and distance between the bubble center and the wall (lower panel) as functions of the number of sound cycles. Initially the bubble is located at a distance of 2 mm from the plane wall. The bubble radius is normalized by the linear resonance value R_{res} which is 75 μm in this case; the initial radius is 35 μm. The sound frequency is 20 kHz, the acoustic pressure amplitude 0.3 atm, and the liquid water in saturated conditions at 1 atm and 100 °C. The acoustic wave fronts are parallel to the wall.

Fig. 4 is for an initial separation of 2 mm from the wall and Fig. 5 for 1 mm.

If the liquid superheat is greater, the bubble will go through resonance earlier[43] and therefore it might escape from the wall even when it is released somewhat closer to it, and conversely in a subcooled liquid. In both cases, however, the general behavior would remain qualitatively unchanged.

In the present model the bubble is forced to remain spherical and the computation must stop when it touches the wall. It appears likely that in practice one would observe a flattening of the bubble against the wall under the action of the secondary Bjerknes force. The question remains of whether, once the bubble has grown past the resonance radius, the primary Bjerknes force is strong enough to overcome the secondary Bjerknes force. In order to explore this point, within the framework of the present model, it is necessary to prevent the bubble from touching the wall as it grows beyond the resonance radius. We achieve this objective simply by keeping the bubble center fixed when it reaches a distance from the wall close to the resonance radius. We have conducted a number of numerical experiments in this way varying the acoustic pressure amplitude and other parameters, but we have invariably found that the primary Bjerknes force is too weak to overcome the attractive secondary force and the bubble is never able to leave the neighborhood of the wall.

In the previous examples the wall was modeled as rigid which, since $\nabla P=0$ at the wall, has the effect of reducing the magnitude of the primary Bjerknes force in the very region where it is most needed. One may investigate the qualitative effect of a slightly compliant surface by using, in place of (4.1), the modified pressure field

$$P_A = P_a \sin \omega t \cos(kz+\phi), \tag{4.2}$$

where the phase ϕ is introduced to account for the acoustic impedance of the wall. If ϕ is positive, the (virtual) pressure antinode is located at a distance $(c/\omega)\phi$ below the wall while, for negative ϕ, the antinode is real and located at an equal distance above the wall. If $\phi>0$, the liquid acceleration as deduced from (4.2) is positive for $P_A>0$, which

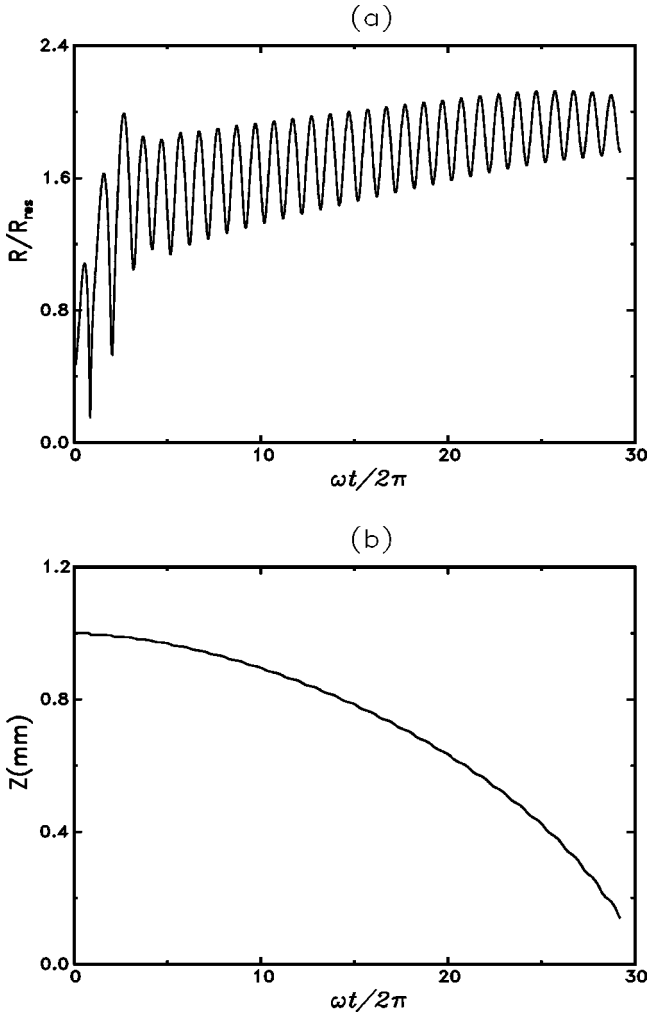

FIG. 5. The same as in Fig. 4 for an initial bubble position 1 mm from the wall.

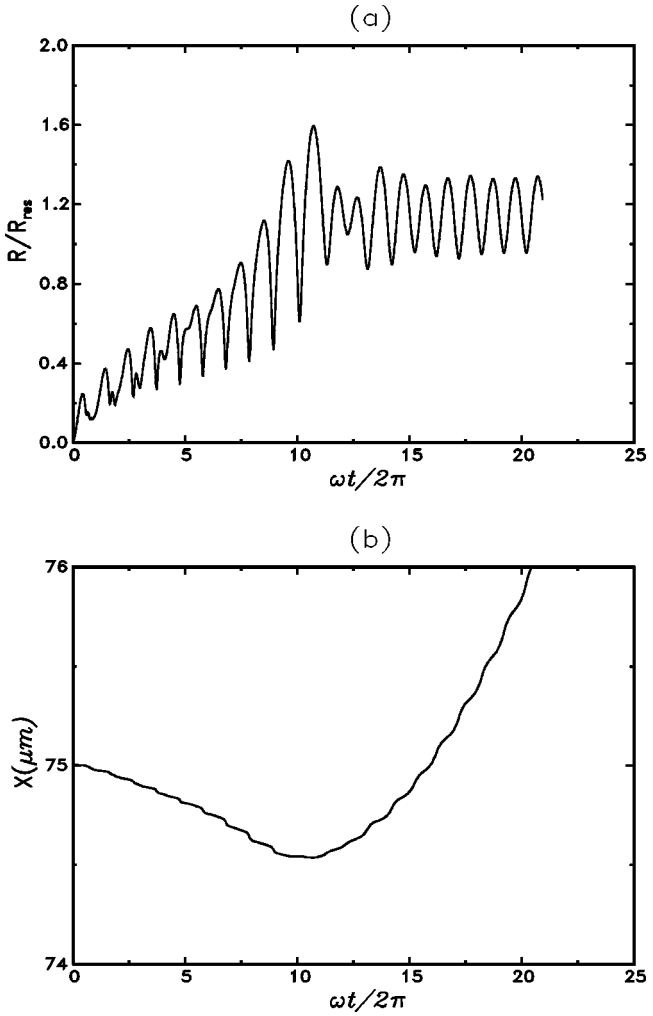

FIG. 6. Distance of the bubble from the pressure antinode for the case of sound wave fronts normal to a plane wall as a function of the number of sound cycles. The bubble is placed initially 75 μm away from the pressure antinode at 4.4 mm from the wall; the water is saturated at 100 °C and 1 atm, the initial radius is 35 μm, the pressure amplitude is 0.4 atm, and the sound frequency 1 kHz.

implies that the wall moves in phase with the pressure. This would be the case for a ''hard'' wall driven below its natural frequency. Conversely, for $\phi<0$, one deals with a ''soft'' wall. Our numerical results show that, in the former case, for ϕ in the range 0 to 0.1π, the behavior is qualitatively the same as shown in Fig. 1. As ϕ is gradually increased, due to the corresponding increase in the local pressure gradient, the distance from the wall at which bubbles start to be repelled becomes smaller and smaller, but the practical implication of this fact is probably not very interesting as materials that have at the same time good heat conductivity and a sufficiently low impedance to result in a relatively large ϕ probably do not exist. For negative ϕ, the presence of a pressure antinode above the wall has the effect of reversing the bubble behavior: the force is away from the wall below resonance and toward the wall above. Soft walls would therefore be completely unsuitable.

These numerical experiments suggest that it would be very difficult if not impossible to drive boiling bubbles away from a heated wall by using a sound field with wave fronts parallel to the wall. Another option, that we explore in Sec. V, is to arrange the sound field in such a way that the wave fronts are normal to the wall.

V. RESULTS: SOUND WAVE FRONTS NORMAL TO THE SOLID SURFACE

If bubbles cannot be removed from the wall it may be possible to move them *along the wall* to a region where, for example, they can be entrained in a suitable low-velocity imposed flow. Possible arrangements to achieve this objective will be briefly considered in Sec. VI. With this possibility in mind, we now focus on the description of the bubble motion in the direction parallel to the wall under the action of a sound field with wave fronts perpendicular to the wall. We take the pressure field to be given by

$$P_A = P_a \sin \omega t \cos kx, \tag{5.1}$$

where the coordinate x is measured from the pressure antinode and runs parallel to the solid surface.

As noted before, the attractive effect of the image bubble is powerful and would force the bubble against the solid surface. The tangential component of the primary Bjerknes force would, however, remain unbalanced and would pro-

mote a sliding of the bubble along the wall. As a matter of fact, experimental evidence of this behavior has recently been obtained.[46] Since we cannot allow our bubbles to deform, here again we resort to the same artifice used in Sec. IV and disregard the bubble momentum equation in the direction normal to the wall, maintaining the bubble center at a fixed distance from the wall. In Fig. 6 we show one example. Here the bubble is placed initially 75 μm away from the pressure antinode at 4.4 mm from the wall; the water is saturated at 100 °C and 1 atm, the initial radius is 35 μm, and the pressure amplitude is 0.4 atm. The bubble initially moves toward the pressure antinode, but turns away as it grows past the resonance radius.

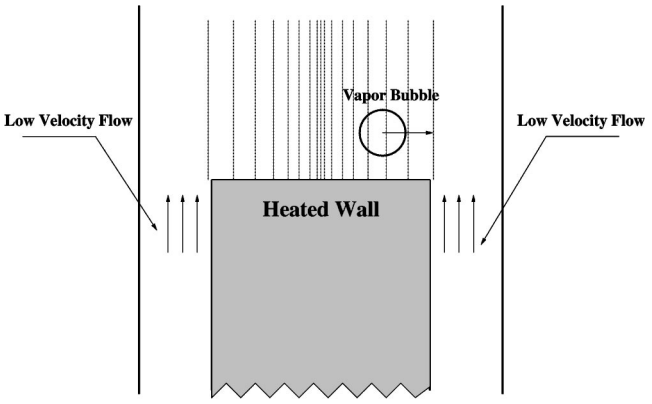

FIG. 7. Illustration of how the mechanism studied in Sec. V can be used for bubble removal by a low velocity liquid stream: The wave fronts are perpendicular to the heated wall, with the pressure antinode near the center. When the bubble grows past its resonant radius, the pressure-radiation force pushes it away from the high-pressure region toward the pressure node, where it can be removed by a suitable low-velocity flow.

VI. CONCLUSIONS

In this work we have studied the behavior of a vapor bubble near a heated wall under the action of an external imposed sound field. The motivation of the work is the necessity to replace buoyancy by some other means for bubble removal under microgravity conditions in order to prevent an early transition to the film boiling regime.

When the acoustic wave fronts are parallel to the wall, the primary pressure-radiation (or Bjerknes) force exerted by the sound tends to drive sufficiently large bubbles away from it. However, due to the presence of the boundary, there is a secondary pressure-radiation force (which may be interpreted as due to the action of an ''image'' bubble), which is strongly attractive and prevents the bubble from leaving the neighborhood of the wall.

As an alternative strategy, we have explored the action of sound fields with wave fronts normal to the wall and we have shown that bubbles can be induced to translate along the wall by such means. We have been led to study this alternative by recent experimental evidence that demonstrates its actual occurrence in practice.[46] By this means, the bubbles can either be removed from the heated region, or they can be pushed to a position where even a slow flow is capable of entraining them and carry them away. A simple arrangement for this purpose is shown in Fig. 7, and many other similar ones can be easily devised. It may be expected that the microconvection caused near the wall by the radial pulsations of the bubbles, as well as their sliding, would contribute to the heat transfer rate. Furthermore, the sound field itself contributes to the bubble growth rate through the process of rectified heat transfer, which will have a beneficial effect on the heat transfer rate from the wall. Although we have presented explicit examples for only two frequencies and in saturated water, a qualitatively identical behavior may be expected in different conditions and with different liquids.

If more than one bubble is present, the mutual Bjerknes forces would promote a coalescence of neighboring bubbles and therefore a more rapid formation of bubbles large enough to be pushed away from the pressure antinode. If the vapor generation rate is very large, there might be a practical difficulty in propagating the sound to the region of interest through the bubbly mixture. Although the computational method that we have presented can be adapted to these and other issues, the amount of required computing would be quite significant and it is possible that an experimental approach might be more effective.

ACKNOWLEDGMENTS

The authors are grateful to Dr. E. Trinh (NASA) and K. Ohsaka (University of Southern California) for sharing with them their experimental observations. They also express their gratitude to NASA for supporting this study under Grant No. NAG3-1924. The analysis of Ref. 49 was first given in Ref. 34.

APPENDIX A

In order to justify the mathematical model of Sec. II we use a singular perturbation argument similar to that of two earlier papers.[47,48]

In the absence of body forces, the continuity and momentum equations for an inviscid compressible liquid are

$$\frac{\partial \rho}{\partial t} + \nabla \cdot (\rho \mathbf{u}) = 0, \tag{A1}$$

$$\rho \left(\frac{\partial \mathbf{u}}{\partial t} + \mathbf{u} \cdot \nabla \mathbf{u} \right) = -\nabla p, \tag{A2}$$

with an equation of state $\rho = \rho(p)$. Let us nondimensionalize these equations according to

$$\mathbf{x} = R_0 \mathbf{x}_*, \quad t = \frac{1}{\omega} t_*, \quad \mathbf{u} = R_0 \omega \mathbf{u}_*,$$

$$p = \omega^2 R_0^2 \rho_L p_*, \quad \rho = \rho_L \rho_*, \tag{A3}$$

where $\rho_L = \rho(P_\infty)$, to find

$$\frac{\partial \rho_*}{\partial t_*} + \nabla_* \cdot (\rho_* \mathbf{u}_*) = 0, \tag{A4}$$

$$\rho_*\left(\frac{\partial \mathbf{u}_*}{\partial t_*}+\mathbf{u}_*\cdot\boldsymbol{\nabla}\mathbf{u}_*\right)=-\boldsymbol{\nabla}_* p_*, \tag{A5}$$

where $\boldsymbol{\nabla}_*$ denotes the gradient operator with respect to the dimensionless coordinate $\mathbf{x}_*$; it is understood that the origin of the coordinate system is the neighborhood of the bubble.

The scaling (A3) is appropriate at distances from the bubble much smaller than the acoustic wavelength, and in this region the bubble radius dictates the length scale. At distances from the bubble comparable with the acoustic wavelength, of the order of c_∞/ω with c_∞ the speed of sound corresponding to P_∞, another scaling for $\mathbf{x}$ is more appropriate:

$$\mathbf{x}=\frac{c_\infty}{\omega}\tilde{\mathbf{x}}. \tag{A6}$$

In terms of $\tilde{\mathbf{x}}$ the previous equations (A1), (A2) become

$$\frac{\partial \rho_*}{\partial t_*}+\epsilon\tilde{\boldsymbol{\nabla}}\cdot(\rho_*\mathbf{u}_*)=0, \tag{A7}$$

$$\rho_*\left(\frac{\partial \mathbf{u}_*}{\partial t_*}+\epsilon\mathbf{u}_*\cdot\tilde{\boldsymbol{\nabla}}\mathbf{u}_*\right)=-\epsilon\tilde{\boldsymbol{\nabla}}p_*, \tag{A8}$$

where $\tilde{\boldsymbol{\nabla}}$ is the gradient operator with respect to $\tilde{\mathbf{x}}$ and

$$\epsilon=\frac{\omega R_0}{c_\infty} \tag{A9}$$

may be considered of the order of the Mach number of the bubble wall radial motion.

To solve (A4) and (A5) we expand the fields in the form

$$\begin{aligned}&\mathbf{u}_*=\mathbf{u}_0+\epsilon\mathbf{u}_1+\cdots,\quad \rho_*=1+\epsilon\rho_1+\cdots,\\ &p_*=p_0+\epsilon p_1+\cdots.\end{aligned} \tag{A10}$$

Upon substitution and separation of orders, the lowest-order problem becomes

$$\boldsymbol{\nabla}_*\cdot\mathbf{u}_0=0, \tag{A11}$$

$$\frac{\partial \mathbf{u}_0}{\partial t_*}+\mathbf{u}_0\cdot\boldsymbol{\nabla}\mathbf{u}_0=-\boldsymbol{\nabla}_* p_0, \tag{A12}$$

i.e., the usual incompressible formulation. These equations should be solved subject to the kinematic and dynamic boundary conditions at the bubble surface and to suitable matching conditions at infinity.

To derive these matching conditions we proceed as in (A10) for the outer equations (A7) and (A8) and expand the flow fields in the outer domain in the form

$$\begin{aligned}&\mathbf{u}_*=\mathbf{U}_0+\epsilon\mathbf{U}_1+\cdots,\quad \rho_*=1+\epsilon R_1++\epsilon^2 R_2\cdots,\\ &p_*=P_0+\epsilon P_1+\cdots.\end{aligned} \tag{A13}$$

When these expansions are substituted into the outer momentum equation (A8), the balance of terms requires that $\mathbf{U}_0=0$. Physically this result depends on the fact that, far from the bubble, liquid motion is primarily induced by the sound field, rather than by the bubble activity, and occurs therefore with a small velocity. As a consequence, the continuity equation (A7) shows that, in the outer field, $\rho_*=1+O(\epsilon)^2$, which is also a known result. With these estimates, (A7) and (A8) give

$$\frac{\partial R_2}{\partial t_*}+\tilde{\boldsymbol{\nabla}}\cdot\mathbf{U}_1=0, \tag{A14}$$

$$\frac{\partial \mathbf{U}_1}{\partial t_*}=-\tilde{\boldsymbol{\nabla}}P_0, \tag{A15}$$

i.e., the acoustic equations. Since $\mathbf{u}_*$ is $O(\epsilon)$ in the far field while p_* is $O(1)$, for $\mathbf{x}_*\to\infty$, the solution of (A11) and (A12) must match to

$$\mathbf{u}_0\to 0,\quad p_0\to P_0, \tag{A16}$$

where P_0 is the inner limit of the imposed sound field. In practice, we can evaluate the sound field in the neighborhood of the origin.

To solve the problem we introduce a harmonic velocity potential, $\mathbf{u}_0=\boldsymbol{\nabla}_*\phi_*$, and integrate the momentum equation (A12) to find the Bernoulli integral in dimensionless form:

$$\frac{\partial \phi_*}{\partial t_*}+\frac{1}{2}\mathbf{u}_0^2+p_0=P_0. \tag{A17}$$

Upon reverting to dimensional variables with the definitions

$$\begin{aligned}&\phi=\omega R_0^2\phi_*,\quad \mathbf{u}=\omega R_0\mathbf{u}_0,\quad P_L=\omega^2 R_0^2\rho_L p_0,\\ &P_\infty+P_A=\omega^2 R_0^2\rho_L P_0,\end{aligned} \tag{A18}$$

this equation becomes (2.2).

APPENDIX B

The convection term in the energy equation (3.2) is expressed in terms of the auxiliary quantity F_C defined by

$$F_C=\frac{1}{\mathcal{N}_{NM}^2}\int_0^\pi \sin\theta\, d\theta\int_0^{2\pi} d\phi\, Y_N^M(\theta,\phi)(\mathbf{u}\cdot\boldsymbol{\nabla}T), \tag{B1}$$

where

$$\begin{aligned}\mathcal{N}_{NM}^2&=\int_0^\pi \sin\theta\, d\theta\int_0^{2\pi} d\phi\,|Y_N^M(\theta,\phi)|^2\\ &=\frac{2(1+\delta_{M0})\pi}{2N+1}\frac{(N+M)!}{(N-M)!}.\end{aligned} \tag{B2}$$

The explicit expression of F_C is

$$F_C=\sum_{n=0}^{\infty}\sum_{m=0}^{n}\sum_{N'=0}^{\infty}\sum_{M'=0}^{N'}\left\{\frac{\partial f_{nm}}{\partial r}\frac{\partial T_{N'M'}}{\partial r}\langle Y_N^M|Y_{N'}^{M'}|Y_n^m\rangle+\frac{\partial f_{nm}}{\partial r}\frac{\partial \tilde{T}_{N'M'}}{\partial r}\langle Y_N^M|\tilde{Y}_{N'}^{M'}|Y_n^m\rangle+\frac{\partial f_{nm}}{\partial r}\frac{\partial T_{N'M'}}{\partial r}\langle \tilde{Y}_N^M|Y_{N'}^{M'}|\tilde{Y}_n^m\rangle\right.$$
$$+\frac{\partial \tilde{f}_{nm}}{\partial r}\frac{\partial \tilde{T}_{N'M'}}{\partial r}\langle Y_N^M|\tilde{Y}_{N'}^{M'}|\tilde{Y}_n^m\rangle+\frac{f_{nm}T_{N'M'}}{r^2}\left\langle Y_N^M\left|\frac{\partial Y_{N'}^{M'}}{\partial\theta}\right|\frac{\partial Y_n^m}{\partial\theta}\right\rangle+\frac{\tilde{f}_{nm}T_{N'M'}}{r^2}\left\langle Y_N^M\left|\frac{\partial Y_{N'}^{M'}}{\partial\theta}\right|\frac{\partial \tilde{Y}_n^m}{\partial\theta}\right\rangle$$
$$+\frac{f_{nm}\tilde{T}_{N'M'}}{r^2}\left\langle Y_N^M\left|\frac{\partial \tilde{Y}_{N'}^{M'}}{\partial\theta}\right|\frac{\partial Y_n^m}{\partial\theta}\right\rangle+\frac{\tilde{f}_{nm}\tilde{T}_{N'M'}}{r^2}\left\langle Y_N^M\left|\frac{\partial \tilde{Y}_{N'}^{M'}}{\partial\theta}\right|\frac{\partial \tilde{Y}_n^m}{\partial\theta}\right\rangle+\frac{mM'f_{nm}T_{N'M'}}{r^2}\left\langle Y_N^M\left|\frac{\tilde{Y}_{N'}^{M'}}{\sin\theta}\right|\frac{\tilde{Y}_n^m}{\sin\theta}\right\rangle$$
$$-\frac{mM'\tilde{f}_{nm}T_{N'M'}}{r^2}\left\langle Y_N^M\left|\frac{Y_{N'}^{M'}}{\sin\theta}\right|\frac{\tilde{Y}_n^m}{\sin\theta}\right\rangle-\frac{mM'f_{nm}\tilde{T}_{N'M'}}{r^2}\left\langle Y_N^M\left|\frac{\tilde{Y}_{N'}^{M'}}{\sin\theta}\right|\frac{Y_n^m}{\sin\theta}\right\rangle$$
$$\left.+\frac{mM'\tilde{f}_{nm}\tilde{T}_{N'M'}}{r^2}\left\langle Y_N^M\left|\frac{Y_{N'}^{M'}}{\sin\theta}\right|\frac{Y_n^m}{\sin\theta}\right\rangle\right\}\frac{1}{\mathcal{N}_{NM}^2},\tag{B3}$$

where $\langle a(\theta,\phi)|b(\theta,\phi)|c(\theta,\phi)\rangle$ involves a scalar product over the unit sphere defined by

$$\langle a(\theta,\phi)|b(\theta,\phi)|c(\theta,\phi)\rangle=\int_0^{\pi}\sin\theta\,d\theta\int_0^{2\pi}d\phi\,a(\theta,\phi)b(\theta,\phi)c(\theta,\phi).\tag{B4}$$

These integrals are related to Wigner's $3-j$ symbols but it has proven more efficient to calculate them numerically by means of Simpson's rule with 501 points.

[1] R. Siegel, ''Effects of reduced gravity on heat transfer,'' in *Advances in Heat Transfer*, edited by J. P. Hartnett and T. F. Irvine, Jr. (Academic, New York, 1967), Vol. 4, pp. 143–228.

[2] J. A. Clark, ''Gravic and agravic effects in cryogenic heat transfer,'' in *Advances in Cryogenic Heat Transfer — Chemical Engineering Progress Symposium*, edited by K. J. Bell (American Institute of Chemical Engineers, New York, 1968), Vol. 64, pp. 93–102.

[3] M. Zell, J. Straub, and B. Vogel, ''Pool boiling under microgravity,'' PCH **11**, 813 (1989).

[4] T. Oka, Y. Abe, K. Tanaka, Y. H. Mori, and A. Nagashima, ''Observational study of pool boiling under microgravity'' JSME Int. J., Ser. II **35**, 280 (1992).

[5] R. Siegel and E. G. Keshock, ''Effects of reduced gravity on nucleate boiling bubble dynamics in saturated water,'' AIChE J. **10**, 509 (1964).

[6] J. S. Ervin, H. Merte, Jr., R. B. Keller, and K. Kirk, ''Transient pool boiling in microgravity,'' Int. J. Heat Mass Transf. **35**, 659 (1992).

[7] J. N. Chung, ''Bubble dynamics, two-phase flow, and boiling heat transfer in a microgravity environment,'' in Second Microgravity Fluid Physics Conference, edited by B. S. Singh, NASA No. 3276, 1994, pp. 259–264.

[8] T. J. Snyder, J. N. Chung, and J. B. Schneider, ''Competing effects of dielectrophoresis and buoyancy on nucleate boiling and an analogy with variable gravity boiling results,'' J. Heat Transfer **120**, 371 (1998).

[9] H. J. Cho, I. S. Kang, Y. C. Kweon, and M. H. Kim, ''Numerical study of the behavior of a bubble attached to a tip in a nonuniform field,'' Int. J. Multiphase Flow **24**, 479 (1998).

[10] C. Herman, ''Experimental investigation of pool boiling heat transfer enhancement in microgravity in the presence of electric fields,'' Proceedings of the Fifth Microgravity Fluid Physics and Transport Phenomena Conference, NASA, 2000, pp. 9–10.

[11] L. A. Crum and A. I. Eller, ''Motion of bubbles in a stationary sound field,'' J. Acoust. Soc. Am. **48**, 181 (1970).

[12] L. A. Crum and D. A. Nordling, ''Velocity of transient cavities in an acoustic stationary wave,'' J. Acoust. Soc. Am. **52**, 294 (1972).

[13] L. A. Crum, ''Acoustic force on a liquid droplet in an acoustic stationary wave,'' J. Acoust. Soc. Am. **50**, 157 (1971).

[14] L. A. Crum, ''Bjerknes forces on bubbles in a stationary sound field,'' J. Acoust. Soc. Am. **57**, 1363 (1975).

[15] E. M. Agrest and G. N. Kuznetsov, ''Migration of gas-filled cavities in an inhomogeneous sound field,'' Sov. Phys. Acoust. **18**, 143 (1972).

[16] E. M. Agrest and G. N. Kuznetsov, ''Instantaneous parameters of the motion of a cavitation bubble in an inhomogeneous sound field,'' Sov. Phys. Acoust. **19**, 212 (1973).

[17] M. A. H. Weiser and R. E. Apfel, ''Extension of acoustic levitation to include the study of micron-size particles in a more compressible host liquid,'' J. Acoust. Soc. Am. **71**, 1261 (1982).

[18] M. Barmatz and P. Collas, ''Acoustic radiation potential on a sphere in plane, cylindrical, and spherical standing wave fields,'' J. Acoust. Soc. Am. **77**, 928 (1985).

[19] E. H. Trinh and C. J. Hsu, ''Acoustic levitation methods for density measurements,'' J. Acoust. Soc. Am. **80**, 1757 (1986).

[20] R. G. Holt and L. A. Crum, ''Acoustically forced oscillations of air bubbles in water: Experimental results,'' J. Acoust. Soc. Am. **91**, 1924 (1992).

[21] C. P. Lee and T. G. Wang, ''Acoustic radiation force on a bubble,'' J. Acoust. Soc. Am. **93**, 1637 (1993).

[22] T. Barbat, N. Ashgriz, and C. G. S. Liu, ''Dynamics of two interacting bubbles in an acoustic field,'' J. Fluid Mech. **389**, 137 (1999).

[23] K. Yosioka and Y. Kawasima, ''Acoustic radiation pressure on a compressible sphere,'' Acustica **5**, 167 (1955).

[24] A. I. Eller, ''Force on a bubble in a standing acoustic wave,'' J. Acoust. Soc. Am. **43**, 170 (1986).

[25] J. M. Foster, J. A. Botts, A. R. Barbin, and R. T. Vachon, ''Bubble trajectories and equilibrium levels in vibrated liquid columns,'' J. Basic Eng. **90**, 125 (1968).

[26] R. Löfsted and S. Putterman, ''Theory of long wavelength acoustic radiation pressure,'' J. Acoust. Soc. Am. **90**, 2027 (1991).

[27] C. P. Lee and T. G. Wang, ''Acoustic radiation force on a bubble,'' J. Acoust. Soc. Am. **93**, 1637 (1993).

[28] T. J. Asaki and P. L. Marston, ''Acoustic radiation force on a bubble driven above resonance,'' J. Acoust. Soc. Am. **96**, 3096 (1994).

[29] M. S. Plesset and R. B. Chapman, ''Collapse of an initially spherical vapour cavity in the neighbourhood of a solid boundary,'' J. Fluid Mech. **47**, 283 (1971).

[30] W. Lauterborn and H. Bolle, ''Experimental investigations of cavitation-bubble collapse in the neighborhood of a solid boundary,'' J. Fluid Mech. **72**, 391 (1975).

[31] H. Yuan and A. Prosperetti, ''Gas-liquid heat transfer in a bubble collapsing near a wall,'' Phys. Fluids **9**, 127 (1997).

[32] A. S. Sangani and C. Yao, ''Bulk thermal conductivity of composites with spherical inclusions,'' J. Appl. Phys. **63**, 1334 (1988).

[33] A. S. Sangani and R. Sureshkumar, ''Linear acoustic properties of bubbly

liquids near the natural frequency of the bubbles using numerical simulations,'' J. Fluid Mech. **252**, 239 (1993).
[34]M. Watanabe, ''Topics in bubbly liquid flows and cavitation,'' Ph.D. thesis, Johns Hopkins University, 1995.
[35]A. Prosperetti, ''The thermal behaviour of oscillating gas bubbles,'' J. Fluid Mech. **222**, 587 (1991).
[36]D. E. Hagen, J. Schmitt, M. Trueblood, Carstens, D. R. White, and D. J. Alofs, ''Condensation coefficient measurement for water in the UMR cloud simulation chamber,'' J. Atmos. Sci. **46**, 803 (1989).
[37]M. Kotani, T. Tsuzuyama, Y. Fujii, and S. Fujikawa, ''Nonequilibrium vapor condensation in shock tube,'' JSME Int. J., Ser. B **41**, 436 (1998).
[38]N. S. Khabeev, ''Heat transfer and phase-transition effects in the oscillation of vapor bubbles,'' Sov. Phys. Acoust. **21**, 501 (1976).
[39]N. A. Gumerov, ''Weakly non-linear oscillations of the radius of a vapour bubble in an acoustic field,'' J. Appl. Math. Mech. **55**, 205 (1991).
[40]N. A. Gumerov, ''Dynamics of vapor bubbles with non-equilibrium phase transitions in isotropic acoustic fields,'' Phys. Fluids **12**, 71 (2000).
[41]T. Tsuruta and G. Nagayama, ''A molecular dynamics approach to interphase mass transfer between liquid and vapor,'' in *Heat Transfer and Transport Phenomena in Microsystems*, edited by G. P. Celata, V. P. Carey, M. Groll, and I. Tanasawa (Kluwer, Dordrecht, 2001).
[42]D. A. Labuntsov and A. P. Kryukov, ''Analysis of intensive evaporation and condensation,'' Int. J. Heat Mass Transf. **22**, 989 (1979).
[43]Y. Hao and A. Prosperetti, ''The dynamics of vapor bubbles in acoustic pressure fields,'' Phys. Fluids **11**, 2008 (1999).
[44]R. I. Nigmatulin, N. S. Khabeev, and Z. N. Hai, ''Waves in liquids with vapour bubbles,'' J. Fluid Mech. **186**, 85 (1988).
[45]Y. Hao and A. Prosperetti, ''The collapse of vapor bubbles in a spatially non-uniform flow,'' Int. J. Heat Mass Transf. **43**, 3539 (2000).
[46]K. Ohsaka and E. H. Trinh (private communication).
[47]A. Prosperetti and A. Lezzi, ''Bubble dynamics in a compressible liquid. Part 1. First-order theory,'' J. Fluid Mech. **185**, 289 (1986).
[48]A. Lezzi and A. Prosperetti, ''Bubble dynamics in a compressible liquid. Second-order theory,'' J. Fluid Mech. **185**, 289 (1987).
[49]See EPAPS Document No. E-PHFLE6-13-009105 for a numerical method for many-bubble interaction. This document may be retrieved via the EPAPS homepage (http://www.aip.org/pubservs/epaps.html) or from ftp.aip.org in the directory /epaps/. See the EPAPS homepage for more information.